Millisecond microwave spikes: statistical study and application for plasma diagnostics

I. V. Rozhansky[1,2], G. D. Fleishman[3,2], G.-L. Huang[1]

ABSTRACT

We analyze a dense cluster of solar radio spikes registered at 4.5 – 6 GHz by the Purple Mountain Observatory spectrometer (Nanjing, China) operating in the 4.5 – 7.5 GHz range with the 5 ms temporal resolution. To handle with the data from the spectrometer we developed a new technique utilizing a nonlinear multi-Gaussian spectral fit based on chi-squared criteria to extract individual spikes from the originally recorded spectra. Applying this method to the experimental raw data we eventually identified about 3000 spikes for this event, which allows for a detailed statistical analysis. Various statistical characteristics of the spikes have been evaluated, including intensity distributions, spectral bandwidth distributions, and distribution of the spike mean frequencies. The most striking finding of this analysis is distributions of the spike bandwidth, which are remarkably asymmetric. To reveal the underlaying microphysics we explore the local trap model with the renormalized theory of spectral profile of the electron cyclotron maser (ECM) emission peak in a source with random magnetic irregularities. The distribution of the solar spikes relative bandwidth calculated within the local trap model represents an excellent fit to the experimental data. Accordingly, the developed technique may offer a new tool of studying very low levels of the magnetic turbulence in the spike sources, when the ECM mechanism of the spike cluster is confirmed.

Subject headings: acceleration of particles — Sun: flares — Sun: coherent emission—Sun: radio radiation

[1]Purple Mountain Observatory, National Astronomical Observatories, Nanjing 210008, P.R. China

[2]Ioffe Institute for Physics and Technology, 194021 St.Petersburg, Russia

[3]New Jersey Institute of Technology, Newark, NJ 07102

1. Introduction

Solar radio spikes are known to be very narrowband kind of solar radio emission (Benz 1985; Stähli and Magun 1986) displaying a typical bandwidth of the order of 1%. A more detailed study of the bandwidth distribution and its correlations with other observed parameters was performed by Csillaghy and Benz (1993). They noted that the bandwidth changes significantly from one event to another, so no clear correlation between the bandwidth and the observing frequency is visible. Thus, the bandwidth is more characteristics of the event rather than function of frequency.

Then, no unique correlation between the bandwidth and radio flux of the spikes was found: there were uncorrelated cases, as well as correlated and anti-correlated cases. Based on these results, Csillaghy and Benz (1993) concluded that the observed bandwidth is formed mainly by source inhomogeneity rather than natural bandwidth of the underlying emission process.

Messmer and Benz (2000) applied a more advanced approach to determine a minimum bandwidth of solar radio spikes, assuming that the minimum bandwidth may correspond to the natural bandwidth of the emission process, while broader spikes are signature of the source inhomogeneity. The minimum bandwidth for two considered events was 0.17% and 0.41% respectively, implying the natural bandwidth of the emission process to be less than the measured values.

The currently available data about the radio spikes appearing at the main flare phase are pretty consistent with the idea that the source of spike cluster is a loop filled by fast electrons and relatively tenuous background plasma (Fleishman et al. 2003). The trapped fast electrons have a nonthermal (power-law) energy spectrum and a loss-cone angular distribution. Each single spike is generated in a local source inside this loop when the local anisotropy is increased compared with the averaged one to produce electron cyclotron maser (ECM) emission. The assumed fluctuations of the pitch-angle distribution of fast electrons can be produced by the magnetic turbulence like in the turbulent model proposed by (Barta and Karlicky 2001).

ECM emission is believed to be responsible for many kinds of solar, planetary and stellar radiation (Stepanov 1978; Wu and Lee 1979; Holman et al. 1980; Melrose and Dulk 1982; Sharma and Vlahos 1984; Wu 1985; Winglee et al. 1988; Aschwanden and Benz 1988; Aschwanden 1990; Barrow et al. 1994; Stupp 2000; Vlasov et al. 2002; LaBelle and Treumann 2002; Treumann 2006). Recently (Fleishman and Melnikov 1998; Fleishman et al. 2003), new important evidence for solar radio spikes to be produced by ECM emission has been obtained. However, although ECM emission fits well to many spike properties, no direct

comparison between the spike spectral properties and the ECM spectral properties has been made yet.

Hewitt et al. (1982) suggested a simple kinematic estimate for the ECM bandwidth

$$\Delta\omega/\omega \sim (v/c)^2, \tag{1}$$

where ω is the central frequency of the emission line, $\Delta\omega$ is the spectral bandwidth, v is a characteristic velocity of fast particles responsible for the ECM generation. This estimate has evidently a limited applicability region, since it does not depend on fast electron pitch-angle distribution, viewing angle etc. Moreover, it is not clear what value of v should be used if the energy distribution of fast electrons is rather broad like in case of power-law spectra typical for solar flares.

The problem of ECM bandwidth attracted a lot attention in connection with the fine structure of the terrestrial auroral kilometric radiation (AKR) (Gurnett and Anderson 1981; Baumback and Calvert 1987; Yoon and Weatherwax 1998; Pritchett et al. 1999). Indeed, the bandwidth of individual AKR peaks is observed to be as small as $\Delta\omega/\omega \sim 10^{-3}$ (Gurnett and Anderson 1981) with the extreme values down to 10^{-5} (Baumback and Calvert 1987). It was shown recently (Yoon and Weatherwax 1998) that the choice of a realistic distribution function of the superthermal electrons may easily provide the ECM bandwidth of the order of 10^{-3}.

However, the results obtained for the auroral region cannot be directly applied to the solar case because of important differences in the source conditions. First of all, the plasma frequency to gyrofrequency ratio

$$Y = \omega_{pe}/\omega_{Be} \tag{2}$$

is much less than unity for the AKR source, while is of the order of unity or larger for the solar corona. Therefore, the corrections to the wave dispersion provided by superthermal electrons may be important for the AKR source (Yoon and Weatherwax 1998), while are typically negligible for the solar case. Then, the fundamental extraordinary wave-mode is the most important if $Y \ll 1$, while different wave-modes (fundamental or harmonic ordinary and harmonic extraordinary) become important if $Y \sim 1$. The distributions of the fast electrons are also believed to differ significantly for these two cases: keV electrons are responsible for the AKR, while broad distributions covered the range $10 - 10^3$keV at least arise typically in solar flares.

Thus, the study of the ECM spectral properties for the conditions typical for solar flares is largely an independent problem that deserves particular attention and careful theoretical consideration. So far, the natural bandwidth of the ECM emission in the standard coronal

conditions has been studied in detail by Fleishman (2004a) who demonstrated that the relative ECM bandwidth typically belongs to the range

$$\Delta\omega/\omega \sim 0.1 - 0.4\%, \tag{3}$$

which is more than one order of magnitude less than intuitive estimate (1).

The effect of source inhomogeneity on the bandwidth of ECM peaks was studied by Platonov and Fleishman (2001) in the linear approximation, i.e., when the quasilinear saturation and nonlinear wave-wave interactions are not important. The corresponding broadening related to gradual non-uniformity of the solar corona was found to be rather small, while the effect of *random* inhomogeneities of the magnetic field is typically important. Fleishman (2004b) developed a renormalized theory of the ECM emission in the source with random inhomogeneities of the magnetic field and found that relatively weak magnetic inhomogeneities can provide strong broadening of the ECM peaks.

In this paper we analyze a dense cluster of solar radio spikes registered at high frequencies above 4.5 GHz. A special numerical technique was developed to decompose partly overlapping spikes in the cluster into individual gaussian spikes and yield large statistically significant series of the spikes. Applying this method to the experimental raw data we eventually identified about 3000 spikes for the observed event, which allows for a detailed statistical analysis.

The most striking finding of this analysis is distributions of the spike bandwidth, which are remarkably asymmetric. The overall bandwidth distribution has a characteristic skew shape with rapid increase at low values of the relative bandwidth followed by maximum at 0.6 % and smooth tail approaching zero at approximately 3%. In order to account for the essential features of the bandwidth distributions we explicitly use the renormalized theory of spectral profile of the ECM emission peak. The theory accurately takes into account the fluctuations of the magnetic field in the spike source. The bandwidth distribution obtained by the proposed theory is found to agree excellently with the observed spike bandwidth distribution.

2. Observations

We analyze a dense cluster of solar radio spikes registered from 05:18:03-05:18:09 UT on April, 10, 2001, at 4.5 – 6 GHz by the Purple Mountain Observatory spectrometer (Nanjing, China) operating in the 4.5 – 7.5 GHz range with the temporal resolution of 5 ms. The cluster occurred during a X2.3 flare on April 10, 2001 (Asai et al. 2003; Chernov et al. 2006), NOAA region 9415, located close to the center of the solar disk (S23W06-08). The

flare was associated with a halo CME, meter-wavelength types II and IV bursts, and strong microwave continuum burst.

The spike cluster occurred during a local impulsive peak of strong long microwave burst with the absolute peak value in excess of 6000 sfu around 9.4 GHz. Highly polarized coherent emissions (LCP at 2 GHz and RCP at 3.75 GHz) were recorded by the Nobeyama Polarimeters around the time of the spike cluster. Context data on the photospheric magnetic fields and microwave emission at 17 GHz at the time of spike cluster are shown in Figure 1.

2.1. Instrumentation

The data we use here are collected by the radio spectrometer at PMO, China (Xu et al. 2003). It has 300 frequency channels per 3 GHz band of 4.5-7.5 GHz with spectral resolution of 10 MHz and time resolution of 5 ms, which observes daily between 1:00 and 9:00 UT.

The dynamic spectrum measured for the event studied is given in Figure 2(a). Two most intensive regions of the spike cluster can be seen around the second and the third seconds of the given dynamic spectrum. As seen from the figure the spikes are not well separated in the frequency domain but rather substantially overlap producing a continuously fluctuating spectrum.

2.2. Spike Resolution and Identification

If the resolution of the instrument is high enough in both temporal and spectral domains, each spike represents a 2D object in the dynamic spectrum, which can, in particular, be characterized by duration, bandwidth, and spectral drift (Dabrowski et al. 2005). In many cases, however, the resolution in either spectral or temporal domain is insufficient to fully resolve each spike. Let us consider first the available temporal resolution against the spike duration.

Lower-frequency observations performed mainly at the decimetric spectral range show that the spike duration is largely a function of the emission frequency with rather weak scatter around the regression curve (Güdel and Benz 1990; Meszarosova et al. 2002, 2003), see also Figure 3 gathering all currently available measurements of spike duration. The regression law found from this figure for the entire available spectral range, $237 - 2695$ MHz,

$$\tau \propto f^{-1.29\pm0.08}, \tag{4}$$

represents a corrected Güdel-Benz law established by Güdel and Benz (1990) for a limited

spectral range. This law predicts that the duration of spikes at $f > 4.5$ GHz should be less than 2 ms, which is well below the spectrometer temporal resolution, 5 ms.

To check this prediction we studied the cross-correlation of the recorded signal vs time lag and found that the adjacent time frames are indeed entirely uncorrelated, Figure 4. This means that each spike does appear only once in the dynamic spectrum in most of the cases. Therefore, the spikes are not resolved in time by the PMO spectrometer. Thus, each time frame has to be processed independently from the adjacent time frames. This reduces a 2D fitting problem to a sequence of 1D fitting problems, which is much easier task.

On the contrary, the spike signal is well resolved in the spectral domain. Figure 5 shows autocorrelation of the instantaneous spike signal in frequency domain. The autocorrelation functions were calculated for each time frame having firm spike signal. The obtained average autocorrelation function is shown in Figure 5 referenced as 'observed'. The squares connected by the solid line show correlation coefficient calculated at lag values of $n\times10$ MHz where integer n denotes the number of frequency channels of the spectrometer (having spectral resolution of 10 MHz). Significant correlation between a few adjacent channels clearly indicates that each spike is seen through several spectral channels.

To understand the meaning of the shape and bandwidth of the cross-correlation function obtained we performed a very simple modeling as follows. We calculated the autocorrelation function of a pure gaussian signal with a certain bandwidth. The corresponding gaussian signal $g(f)$ is shown in the inset in Figure 5. Remarkably, 'observed' curve can be excellently fitted with the autocorrelation of a purely gaussian signal of a certain width Γ ('modeled' curve in Figure 5). Even though, the similarity of the 'observed' curve to the 'modeled' curve can be a result of the Central Limiting Theorem, rather than a similarity of individual spike profiles to pure gaussian, it, nevertheless, implies the presence of a characteristic bandwidth in the spike signal. The best agreement between the 'modeled' and 'observed' plots is achieved for $\Gamma = 30$ MHz, which suggests that the bandwidth of the majority of the spikes is around 30 MHz.

This value is not at all unexpected. Csillaghy and Benz (1993) studied 196 individual spikes recorded in different events over sufficiently broad spectral range to yield an empirical regression law $\Gamma[MHz] = 0.66 f[MHz]^{0.42}$, which implies $\Gamma \approx 25$ MHz at the frequencies 4.5-6 GHz. Given a very large scatter of individual measurements around this regression curve in (Csillaghy and Benz 1993), we conclude that our finding of the characteristic bandwidth around 30 MHz is in full agreement with the results of Csillaghy and Benz (1993). Dividing this value by the typical frequency of ≈ 5 GHz we get the relative bandwidth of a spike $\Gamma_{rel} \approx 0.6\%$. Thus, we can identify this value of Γ_{rel} with a characteristic relative bandwidth of spikes contained in the measured data.

2.3. Spike Decomposition Technique

To handle with the data from the spectrometer we developed a new technique utilizing a nonlinear multi-Gaussian spectral fit based on chi-squared criteria to extract individual spikes from the originally recorded spectra. At the first stage we reveal the time frames where the intensity of the signal cannot be well distinguished from the noise in the whole frequency range. Such frames are excluded from the further analysis. The retained part of the dynamic spectra with distinguishable spiky signal is shown in Figure 2 (b). The technique described below is sequentially applied to the set of retained time frames. Remind that each instantaneous spectrum is treated as a set of unique independent spikes. The input for the elementary fitting procedure is, therefore, an instantaneous spectrum $S(f_j)$. The signal $S(f_j)$ is fitted with a sum of model spikes superposed on a zero level z, which does not depend on frequency but may change from frame to frame. Each spike is assumed to have a Gaussian shape described by three parameters, namely amplitude (A_i), mean (f_{0i}), and standard deviation (γ_i).

$$S^*(f) = z + \sum_{i=1}^{M} s_i(f), \tag{5}$$

$$s_i(f) = s_i(f, A_i, f_{0i}, \gamma_i) = A_i e^{-\frac{(f-f_{0i})^2}{2\gamma_i^2}}. \tag{6}$$

No frequency-dependent background component besides the statistical noise is assumed. We shall often use the bandwidth Γ_i (full width at half maximum) to describe a spike rather than standard deviation, both values related through $\Gamma_i = 2\sqrt{2\ln 2}\gamma_i \approx 2.35\gamma_i$. It must be noted that the bandwidths derived from the fitting (both Γ_i and γ_i) are arbitrary real numbers rather than integer multiples of the instrument spectral resolution of 10 MHz.

The fitting procedure starts from guess set of M spikes $\{s_{0i}\}$, their number and amplitudes being that of local maxima found in the signal above certain noise-threshold level. We changed this noise-threshold level in various runs of the fitting to check the consistency and stability of the fitting results. The constrained nonlinear minimization is performed with regard to the chi-squared statistics

$$\chi^2 = \sum_j \frac{\left(S(f_j) - S^*(f_j)\right)^2}{\sigma_j^2}. \tag{7}$$

using IDL routine CONSTRAINED_MIN. The residual of this fitting consists generally of the statistical noise (which is presumably known based on the instrument characteristics) and a contribution from numerous weak unresolved spikes, whose contribution is unknown. Thus, the full uncertainties associated with a set of measurements are unknown in advance.

However, if we assume that all measurements have the same standard deviation, σ, and that the model does fit well the data so that $\chi^2 \approx N - 3M$, N is the number of the data points used for the fitting, then we can estimate σ by first assigning an arbitrary constant σ_0 to all points, next fitting for the model parameters by minimizing χ^2, and finally adopting

$$\sigma^2 = \sum_j \frac{\left(S\left(f_j\right) - S^*\left(f_j\right)\right)^2}{N - 3M}. \tag{8}$$

After the minimization procedure is completed, each extracted spike is tested for the statistical significance as follows. The spike is excluded from the fitting function so that

$$S^{**}\left(f\right) = z + \sum_{i=1}^{M-1} s_i\left(f\right). \tag{9}$$

New minimization is performed and the new χ'^2 statistics is calculated keeping the obtained σ. The spike is excluded if this procedure does not decrease the goodness of fit expressed by χ^2 :

$$\frac{\chi'^2}{N - 3(M-1)} \leq \frac{\chi^2}{N - 3M}. \tag{10}$$

Figure 6 shows an example of the fit for three instantaneous spectra taken at the time frames pointed by the arrows in Figure 2(b). The figures show very good agreement between the initial raw signal and the fit spectrum being the sum of the spikes extracted. Figure 6(b) also shows that sometimes the fitting procedure may drop away a spike with a moderate intensity still well pronounced. While such cases are statistically rare, nevertheless we have performed a number of spikes extraction procedures varying the parameters of the constrained minimization as well as the value of the threshold used to get Figure 2(b) from Figure 2(a). The corresponding variation of the output statistical parameters of the extracted spike ensembles allowed us to estimate the statistical errors as well as the mean quantities given in the next subsection.

2.4. Spikes Extraction Results

The developed technique allowed us to extract about 3000 spikes. Each spike i is characterized by its amplitude A_i, mean frequency f_{0i} and the bandwidth Γ_i. The distribution of the spike mean frequencies is shown in Figure 7. In obvious agreement with the raw data spectra (Figure 2 (a),(b)) the number of spikes decreases with the frequency increase. A small deviation from this tendency can be seen near $\approx$ 5 GHz. This corresponds to the sharp end of the first subcluster at about 4.9 GHz and also to the malfunction of a few

frequency channels of the instrument clearly seen as a blue horizontal stripe at ≈ 5.1 GHz in Figure 2 (a). The amplitude distribution of the spikes is shown in Figure 8. Note that only the decreasing part of the distribution has sense while the initial increasing part is possibly an artefact caused by skipping the spikes which undergo the average noise level. The decreasing part of the amplitude distribution follows an exponential law (see the inset in Figure 8), which allows estimation of the number of weak missing spikes to be about 30% of the extracted spikes. The spike amplitude correlates with its frequency as Figure 9 shows, which means that both more spikes and stronger spikes are produced at lower frequencies; the calculated rank correlation coefficient is $r = -0.44$. This tendency is also apparent from Figure 10, which presents the moving average for the spike amplitude versus spike central frequency.

A striking finding of the presented spike analysis is distribution of the spike relative bandwidths. This commonly used dimensionless parameter is defined as spike width at half-maximum divided by the central frequency of the spike. We checked and found that the bandwidth distribution has no imprint of the discretness of the spectral channels: integer multiples of 10 MHz do not display any local peak compared with neighboring non-integer values. All values for the relative bandwidth present in the histogram are in excess the minimum spike bandwidths reported in the literature for other events (Messmer and Benz 2000; Wang et al. 2003).

The distribution of the spike relative bandwidths appears to be remarkably asymmetric. It has a skew shape with rapid increase at low values of the relative bandwidth followed by maximum at 0.6% and smooth tail approaching zero at approximately 3% (Figure 11). Note that the peak of the distribution (0.6%) corresponds to the characteristic spike bandwidth found in §2.2 from the correlation analysis.

The asymmetry of the distribution can be characterized by the skewness which is the third moment:

$$S = \frac{\left\langle (f - f_0)^3 \right\rangle}{\sigma^3}. \tag{11}$$

For the spike ensemble under study the overall skewness is about 1.6. The deviation from the normal distribution is estimated by the forth moment, kurtosis, defined as

$$K = \frac{\left\langle (f - f_0)^4 \right\rangle}{\sigma^4}, \tag{12}$$

which is $K \approx 6$ for our case, in contrast to that of the normal distribution $K_{norm} = 3$. Rather weak correlation is found between amplitude and spike relative bandwidth, Figure 9, the appropriate rank correlation coefficient is only $r \approx -0.2$. No correlation is observed between mean frequency and relative bandwidth of the spikes (the appropriate rank correlation coefficient is $r \approx 0.04$).

The large number of individual spikes identified allows for analysis of the spike properties in restricted spectral regions. Accordingly, we looked for a dependence of the bandwidth distribution shape on the spike central frequency. However, no unambiguous trends have been found. Figure 12 displays the frequency dependence of the moments of the distribution, such as mean, median, standard deviation, skewness, and kurtosis, normalized to the corresponding global values gathered in Table 1. The figure shows no significant deviation of any of these parameters P from its overall average value P_0.

3. Local Trap Model

As has already been noted most of the spike properties are consistent with a local trap model (Fleishman and Melnikov 1998; Fleishman et al. 2003). This model adopts that a spike cluster is produced at a significant portion of a magnetic trap (Figure 13), where a loss-cone distribution of the trapped fast particles is formed due to emptying the loss cone as a result of the electron precipitation into the foot points. The overall pitch-angle anisotropy is moderate on average provided that the mean fast electron distribution is at about the marginal stability state in respect to ECM generation. An important ingredient of the local trap model is a magnetic turbulence, which gives rise to local variation of the fast electron distribution anisotropy. Under favorable conditions, this turbulence will increase the anisotropy to the extent sufficient for the ECM instability to develop at some local places inside the large-scale magnetic trap. Such favorable places represent those local spike sources, quasi-randomly distributed over the trap.

As a byproduct of the key role of the magnetic turbulence in forming the spike local sources, the model suggests that the small-scale end of the magnetic turbulence spectrum persists in each local spike source. Therefore, the spikes are formed in a source, where random magnetic inhomogeneities are superimposed on the mean magnetic field of the source. Fleishman (2004b) developed a theory of the ECM spectral bandwidth taking into account the stochastic irregularities of the magnetic field at the source. He obtained that the bandwidth of a single ECM peak generated in such a source is specified by the relation

$$\Gamma = \Gamma_0 e^{\frac{a}{2\Gamma_0^2}}, \tag{13}$$

where Γ_0 is the "natural" bandwidth of the ECM peak in the uniform source with the optical depth τ in the peak maximum,

$$a = \frac{s_0^2}{2}\frac{\langle \delta B^2 \rangle}{B^2} \tag{14}$$

is a "turbulence parameter", defined by the ECM harmonic number s_0 and the magnetic turbulence energy density $\langle \delta B^2 \rangle / 8\pi$ normalized by the magnetic energy density $B^2/8\pi$. We

note that the magnetic inhomogeneities give rise to quite a strong ECM broadening when $a \gtrsim \Gamma_0^2$. Since $\Gamma_0^2 \ll 1$, rather weak random inhomogeneities of the magnetic field provide large ECM broadening.

To account for the observed spike bandwidth distribution we developed a simple model based on the electron cyclotron maser (ECM) emission within the local source model. Specifically, we make use that the natural spike bandwidth is about $0.1 - 0.3\%$ in agreement with calculations of the ECM natural spectral bandwidth (Fleishman 2004a). We postulate a symmetric gaussian distribution of the natural bandwidth over the spike local sources. Then, we adopt that the turbulent parameter a has another gaussian distribution, not correlated with the natural bandwidth distribution.

Varying the pairs of Γ_0 and a within those two parent distributions we are able to produce artificial sets of spikes. The properties of these artificial spike distributions are specified by the parameters of the adopted gaussian distributions, i.e., mean values and dispersions of Γ_0 and a. In our modeling we kept mean Γ_0 value constant at 0.2% level, while varied a value to study the dependence of the distribution moments on a. The dispersion of both values was taken to be about 15%. An example of the distribution produced by the model is given in Figure 14. Eventually, we generated 50 sets with 3000 artificial spike in each set and calculated four first moments of this distributions, which are plotted in Figure 15.

Figure 15 displays also values of the observed distribution moments. Remarkably, all the observed moment values are consistent with corresponding model values for $a \approx 2 \cdot 10^{-7}$, which is especially important because the model includes only one free parameter to yield all four moments together with the correct values. Saying in other words, the comparison of the observed and model moments offers an elegant method of studying the small-scale magnetic turbulence in the sources of spike clusters. We note that the method is highly sensitive to the magnetic irregularities and capable of detecting the turbulence with remarkably low level $\langle \delta B^2 \rangle / B^2 \sim 10^{-7}$ or even less.

4. Discussion

Although the phenomenon of the narrowband spikes and related fine spectral and temporal structures has not been well understood yet, the permanently accumulated data and its detailed and critical analysis in the context of the competing source models has given rise to a significant progress. In particular, there are currently strong evidences that narrowband millisecond spikes appearing at the main flare phase are generated by ECM emission. It follows, e.g., from detailed comparison between the observed properties of solar radio

spikes and predictions of various theoretical models (Fleishman and Melnikov 1998). Even stronger evidence is found recently from the analysis of correlations between the spikes and accompanying microwave continuum (Fleishman et al. 2003): they found, that spike-producing radio bursts reveal smaller plasma frequency to gyrofrequency ratios than other radio bursts, and the strongest averaged flux of the spike emission is observed when the fast electrons display the hardest energy spectra and the most anisotropic angular distribution.

However, it is still unclear if spikes in all events are produced by the same emission mechanism, or there are different subclasses of the spikes. Indeed, only a half of all spike clusters analyzed by Aschwanden and Güdel (1992) correlate well with simultaneous hard X-ray (HXR) emission, the other half reveal weaker or no correlation. Then, Benz et al. (2002) studied the location of narrowband spikes occurred at frequencies $\lesssim 450$ MHz at the flare decay phase. The spike source was found to be located far away from the main flare location, which was interpreted as a post-flare electron acceleration high in the corona. Such spike bursts are likely different in nature from the spike clusters originating at the impulsive and main flare phase, which are highly correlated with HXR and microwave flare emission. We believe that more progress in understanding the nature of the spikes can be expected when broadband imaging radio instruments start to operate.

Similar dynamic spectra of radio emission produced by different mechanisms can be understood if the (quasi-random) distribution of the spikes in frequency and time is related to the global source structure rather than microscopic emission process. For example, Barta and Karlicky (2001) developed a turbulent model of the spike source, which can result in dynamic spectra typical for spikes for different emission mechanisms. Therefore, detailed case studies as well as statistical studies capable of distinguishing between competing emission mechanisms are exceedingly important.

This paper reports a spike cluster at high frequencies, 4.5–6 GHz, which is relatively rare type of events. No statistics of spikes has been available at this spectral range. To remedy this situation we developed a method capable of extracting spikes from dense clusters of overlapping spikes. Applying this method we extracted a few thousand spikes sufficient for a detailed analysis of spike properties. In particular, besides finding the mean and the variance of the distribution of the spike relative bandwidth, we were able to confidently determine higher moments, namely skewness and kurtosis. We found this distribution to be highly asymmetric and to deviate confidently from the normal distribution. Although similar asymmetric distributions at lower frequencies have already been reported based on manual selections of well isolated gaussian spikes in less dense regions of the spike clusters (Csillaghy and Benz 1993; Messmer and Benz 2000), those previous studies involved much lower numbers of manually selected spikes, therefore, the statistics was less significant.

Complimentary, we developed a simplified theoretical model of spike cluster generation in a magnetic trap with random inhomogeneities based on the renormalized theory of the ECM spectral properties taking into account these inhomogeneities. The simulated spike distribution is remarkably similar to the observed one for this particular event, which is a strong evidence in favor of the ECM mechanism of the spike generation within the local trap model with the magnetic turbulence.

Thus, the demonstrated agreement between the model and observations may suggest a new efficient tool of measuring weak magnetic inhomogeneities in the spike sources. Since the turbulent parameter a depends on the emission harmonics number, it is highly desirable to determine at what harmonics of the gyrofrequency the spikes are produced. A direct answer to this question could be obtained from imaging observations of the spike source, which are currently unavailable at the considered frequency range. Therefore, we have to use some indirect approach.

The ECM emission requires both nonthermal electrons and sufficiently strong magnetic field to coexist at the spike source. Figure 1 displays the photospheric magnetic field regions corresponding to fundamental, second, and third gyroharmonics falling to the 4.5–5.6 GHz range and contours of the optically thin microwave radiation at 17 GHz indicating the region where the fast electrons are present. Although the spikes are produced in the coronal rather than photospheric sources, we believe, that the spatial locations of strong coronal magnetic fields are correlated with regions of strong photospheric magnetic fields. Thus, the presence of strong photospheric magnetic field is a necessary condition for the presence of strong coronal field nearby. Inspection of this figure shows that generation of the fundamental ordinary mode ECM emission is almost certainly excluded, while the fundamental extraordinary ECM emission is not too probable even though it cannot be confidently excluded.

Apparently, the most probable location of the spike source is the position of the peak of the positive Stocks V distribution overlapping with a tongue of the Stocks I distribution occurring on top of the strong positive magnetic field region, because high circular polarization ($\sim$ 50%) of the microwave continuum radiation is a strong indication in favor of large magnetic field in this part of the radio source (Bastian, Benz & Gary 1998). Thus, the second extraordinary harmonics is the most probable emission mode in the spike cluster studied, although the third extraordinary and the second ordinary harmonics cannot be firmly excluded. In any case, the performed study involving the forward modeling offers new sensitive tool of detecting and measuring the magnetic turbulence in the spike sources.

5. Conclusions

We report a high-frequency dense cluster consisting of many overlapping spikes and suggest a tool of decomposing the cluster onto individual gaussian spikes. The large number of the identified spikes allows for much more detailed statistical analysis of them, than has ever been published. Then, we develop a theoretical model of the spikes produced by ECM mechanism in numerous local sources with random magnetic inhomogeneities. We find that the model and the observed distributions of the spike relative bandwidth agree excellently with each other, therefore, the presented observations support the adopted local source model with magnetic turbulence.

Since a specific shape of the model distribution is highly sensitive to the magnetic turbulence, this study suggests an elegant and straightforward way of studying magnetic turbulence in the spike sources. In favorable conditions this study can be performed in the spectral and temporal domains giving rise to the information of the spatial distribution and evolution of the magnetic turbulence. We note that the level of the magnetic turbulence in the considered event is very weak, $a < 10^{-6}$, and most probably not enough for the bulk particle acceleration in the spike source. We interpret this result as an important indication that the spikes are a secondary phenomenon, rather than a manifestation of the primary energy release and particle acceleration.

The developed tool, while powerful and promising, requires further analysis and development. In particular, we need detailed modeling to understand better its capability and limits of applicability to denser spike clusters. This is especially important for studying long-lasting clusters with the spike density strongly changing in time. Then, analysis of larger number of the spike clusters throughout the whole spectral range where the spikes are observed will be necessary to convert this tool into a kind of routine flare diagnostics.

This work was supported in part by NSF grants ATM-0607544 and ATM-0707319 to New Jersey Institute of Technology, by the Russian Foundation for Basic Research, grants No. 06-02-16295, 06-02-16859, 06-02-39029, NFSC projects No. 10333030, 10773032, and 973 program with No. 2006CB806302. We have made use of NASA's Astrophysics Data System Abstract Service, SOHO/MDI data as well as radio data from Nobeyama Radioheliograph and Polarimeters.

REFERENCES

Asai, A., Ishii, T. T., Kurokawa, H., Yokoyama, T., & Shimojo, M. 2003, ApJ, 586, 624

Aschwanden, M.J. 1990, A&AS, 85, 1141

Aschwanden, M.J. and Benz, A.O. 1988, ApJ, 332, 447

Aschwanden, M.J., and Güdel, M. 1992 ApJ, 401, 736

Barrow, C.H., Zarka, P., and Aubier, M.G. 1994 A&A, 286, 597

Bárta, M., and Karlický, M. 2001, A&A, 379, 1045

Bastian, T. S., Benz, A. O., & Gary, D. E. 1998, ARA&A, 36, 131

Baumback, M.M., and Calvert, W. 1987, Geophys. Res. Lett., 14, 119

Benz, A.O. 1985, Sol. Phys., 96, 357

Benz, A.O., Saint-Hilaire, P., and Vilmer, N. 2002, A&A, 383, 678

Chernov, G. P., Sych, R. A., Yan, Y., Fu, Q., Tan, C., Huang, G., Wang, D.-Y., & Wu, H. 2006, Sol. Phys., 237, 397

Csillaghy, A., and Benz, A.O. 1993, ApJ, 274, 487

Dąbrowski, B. P., Rudawy, P., Falewicz, R., Siarkowski, M., & Kus, A. J. 2005, A&A, 434, 1139

Fleishman, G.D. 2004a, Astron. Lett., 30, 603

Fleishman, G.D., 2004b, ApJ, 601, 559

Fleishman, G.D., Gary, D.E., and Nita, G.M. 2003, ApJ, 593, 571

Fleishman, G.D., and Melnikov, V.F. 1998, Physics – Uspekhi, 41, 1157

Gurnett, D. A., and Anderson, R.R.1981, in Physics of Auroral Arc Formation, Geophys. Monogr. ser., Vol. 25, edited by S.-I. Akasofu and J. D. Kan, p. 341, AGU, Washington, D.C.

Güdel, M., and Benz, A.O. 1990, A&A, 231, 202

Hewitt, R.G., Melrose, D.B., and Rönnmark, K.G. 1982, Aust. J. Phys., 35, 447

Holman, G.D., Eichler, D., and Kundu, M.R. 1980, in Radiophysics of the Sun (Eds M.R.Kundu, T.E.Gergely)(Dordrecht: Reidel, 1980) p.457.

LaBelle, J., and Treumann, R.A. 2002, Space Sci. Rev., 101, 295

Lipatov, B.N., Melnikov, V.F., Podstrigach, T.S., Snegirev, S.D., Tikhomirov, Yu.V., Fridman, V.M., and Sheiner, O.A. 2002, Radiophys. and Quantum Electr., 45, 75

Melrose, D.B., and Dulk, G.A. 1982, ApJ, 259, 844

Messmer, P., and Benz, A.O. 2000 A&A, 354, 287

Mészárosová, H., Veronig, A., Zlobec, P., and Karlický, M. 2002 Proc. 10^{th} European Solar Physics Meeting, 'Solar Variability: From Core to Outer Frontiers', Prague, Czech Republic, 9-14 September 2002 (ESA SP-506, December 2002), 1, 347.

Mészárosová, H., Veronig, A., Zlobec, P., and Karlický, M. 2003, A&A, 407, 1115

Platonov, K.Yu., and Fleishman, G.D. 2001, Astron. Repts., 45, 203

Pritchett, P.L., Strangeway, R.J., Carlson, C.W., Ergun, R.E., McFadden, J.P., and Delory, G.T. 1999, J. Geophys. Res., 104, 10317

Sharma, R.R., and Vlahos, L. 1984, ApJ, 280, 405

Stähli, M., and Magun, A. 1986, Sol. Phys., 104, 117

Stepanov, A.V. 1978, Pis'ma v Astron. Zh., 4, 193

Stupp, A. 2000, MNRAS, 311, 251

Treumann, R. 2006, A&A Rev., 13, 229

Vlasov, V.G., Kuznetsov, A.A., and Altyntsev, A.T. 2002, A&A, 382, 361

Wang, M., Wang, K.-Sh., Xu, Ch., Shi, Sh.-B., & Li, W.-H. 2003, Publ. Yunnan Obs., 94, 29

Winglee, R.R., Dulk, G.A., and Pritchett, P.L. 1988, ApJ, 328, 809

Wu, C.S. 1985 Space Sci. Rev., 41, 215

Wu, C.S., and Lee, L.C. 1979 ApJ, 230, 621

Xu, F.-Y., Xu, Z.-C., Huang, G.-L., Yao, Q.-J., Meng, X., & Wu, H.-A. 2003, Sol. Phys., 216, 273

Yoon, P.H., and Weatherwax, A.T. 1998, Geophys. Res. Lett., 25, 4461

Zlobec, P., and Karlický, M. 1998, Sol. Phys., 182, 477

Table 1. Bandwidth distribution parameters

Moment of Distribution	value
Mean (f_0), %	0.91±0.02
Median, %	0.77±0.01
Standard deviation (σ), %	0.55±0.04
Skewness, S	1.6±0.2
Kurtosis, K	5.9±0.6

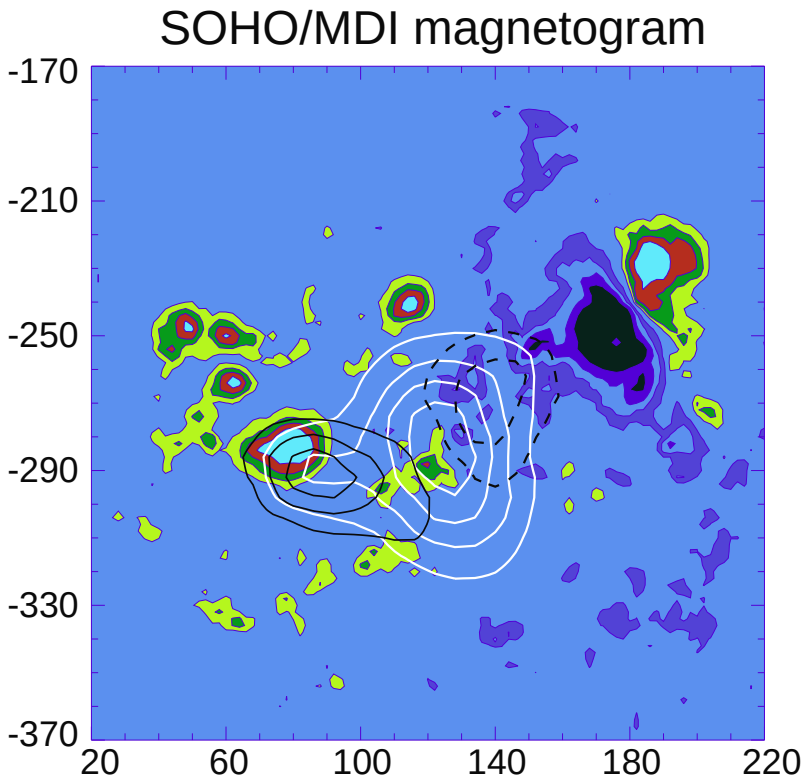

Fig. 1.— Context data at the time of the spike cluster. Color image: SOHO/MDI magnetogram; the contour levels are selected to highlight the photospheric regions where the fundamental gyroharmonics (+1500 to +2000 G, red, and -1500 to -2000 G, violet) and the pair of the second and third harmonics (+500 to +1000 G, yellow, and -500 to -1000 G, dark blue) fall into the 4.5-5.6 GHz spectral range. White contours display the Stocks I distribution at the levels of (0.2, 0.4, 0.6, and 0.8) of I_{max}. Solid black contours display the positive Stocks V distribution (RCP emission) at the levels of (0.05, 0.1, and 0.15) of I_{max}. Dashed black contours display the negative Stocks V distribution (LCP emission) at the levels of (-0.05, and -0.1) of I_{max}.

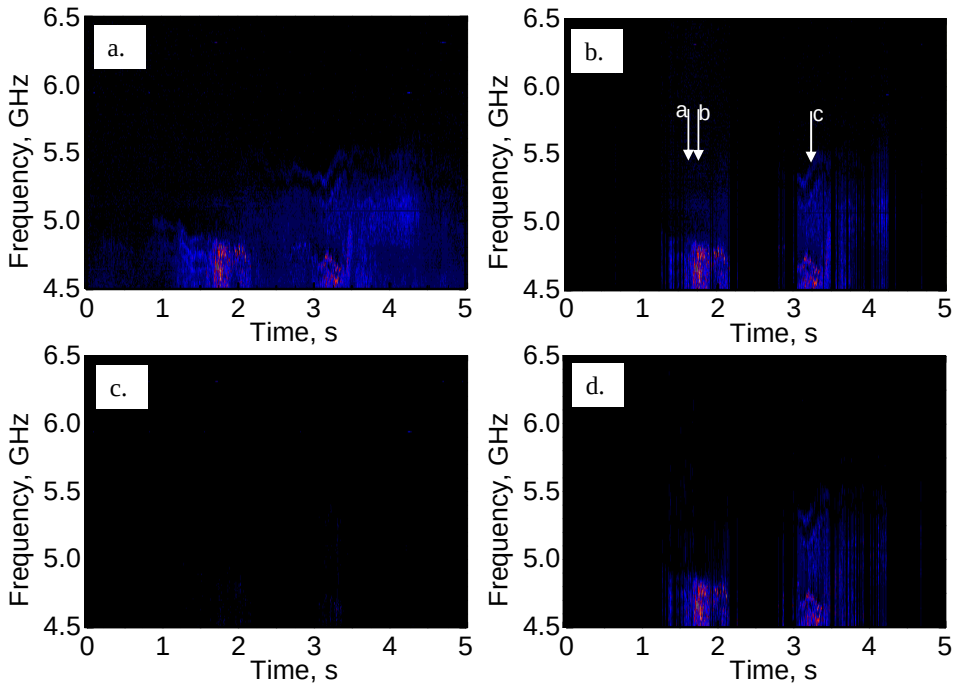

Fig. 2.— Dynamic spectra for the event under study: a – calibrated data from the PMO spectrometer, b – the part of the spectrum selected as input for spikes analysis, d – fitted spectrum obtained by the summation of the extracted Gaussian spikes superimposed on the signal background level, c – the absolute difference between input spectrum (b) and fitted spectrum (d). The arrows in panel (b) point out the time frames expanded in Figure 6. Time is shown in seconds after 05:18:03.5 UT, April, 10, 2001.

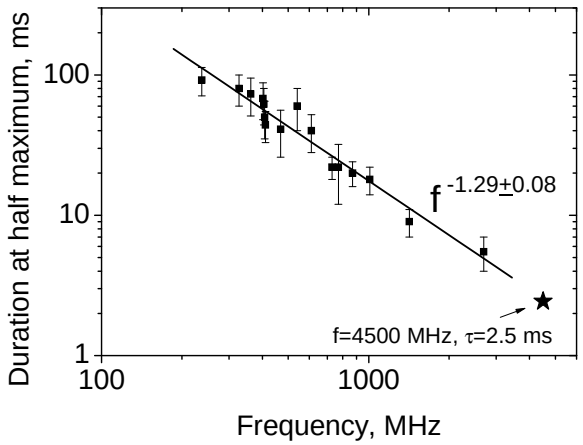

Fig. 3.— Observed duration of spikes at half maximum vs frequency of observation based on published data: 237, 327, 408 and 610 MHz from (Zlobec and Karlicky 1998) and P.Zlobec, private communication, 540 MHz from (Lipatov et al. 2002), 362, 468, 730, 770, 870, 1010 MHz from (Güdel and Benz 1990), and 1420 and 2695 MHz from (Meszarosova et al. 2002, 2003). The solid line is the best power-law fit with the index -1.29 ± 0.08.

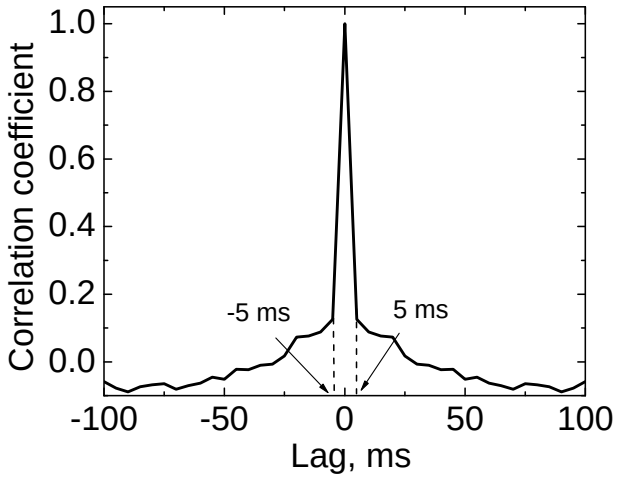

Fig. 4.— Autocorrelation of the variable part of the signal averaged over the frequency channels of the instrument.

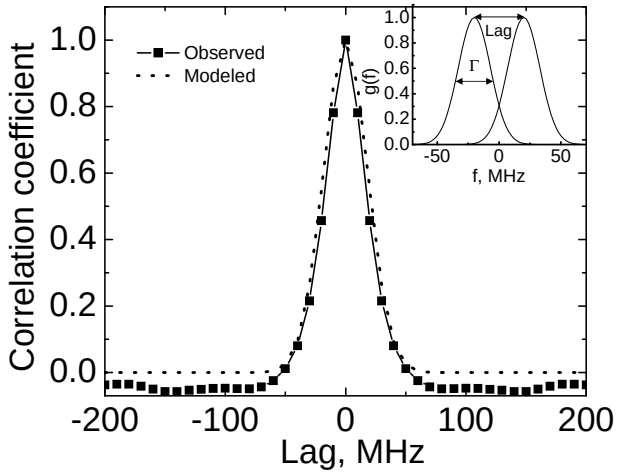

Fig. 5.— Autocorrelation of the instantaneous spectra in frequency domain. The solid line shows the autocorrelation of the measured signal. The squares correspond to the frequency lags equal to integer multiples of the instrumental spectral resolution. The dotted curve represents the best fit with the autocorrelation of a purely gaussian signal $g(f)$ having the bandwidth Γ=30 MHz. The inset shows two instances of the corresponding $g(f)$ shifted by a certain lag.

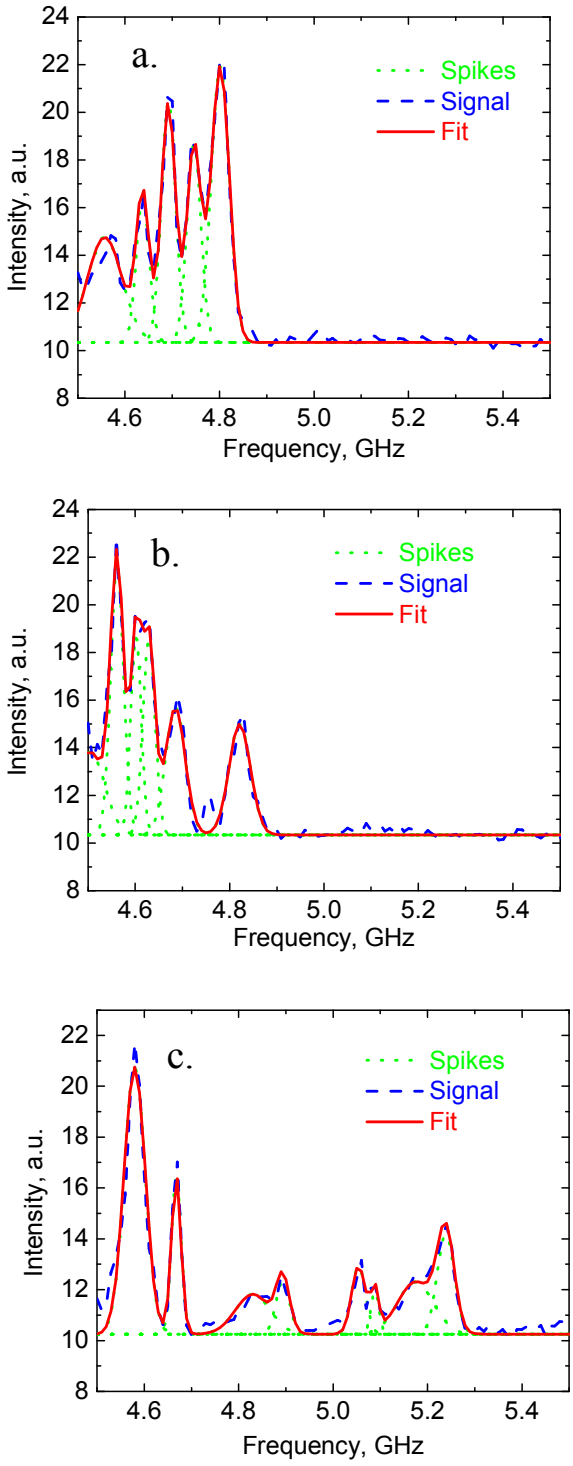

Fig. 6.— Fit examples for three time frames marked by the arrows in Figure 2 (b). Dashed lines represent the input spectra, solid lines are the sums of the extracted spikes. The spikes are shown by dotted line

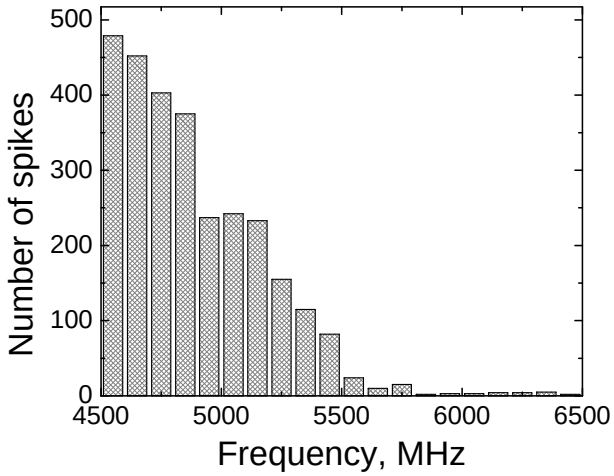

Fig. 7.— Distribution of the mean frequencies of the extracted spikes.

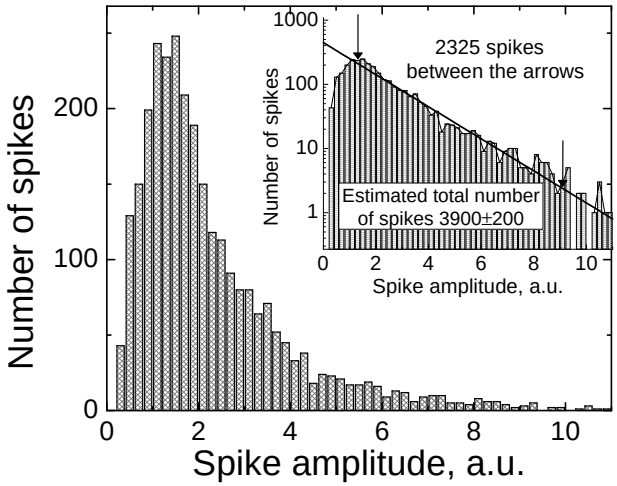

Fig. 8.— Amplitude distribution of the extracted spikes. The inset shows the same distribution in log-linear scale. The solid line is the approximation of the decreasing part of the plot containing 2325 spikes by an exponential distribution. Extrapolation of this line towards zero amplitude allows estimating the total number of the spikes in the time frames selected for the analysis as about 4000.

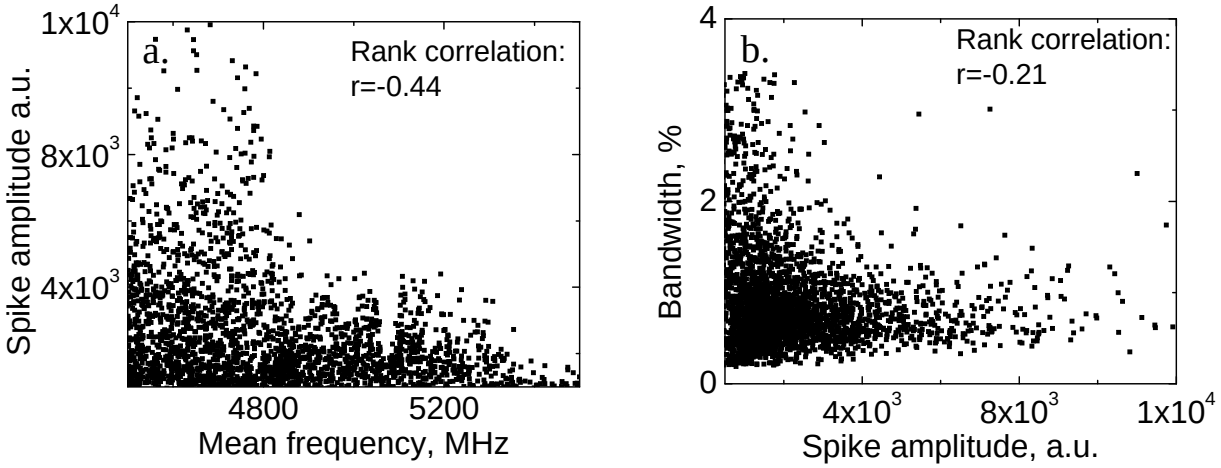

Fig. 9.— Correlation between mean frequency and spike amplitude (left) and between spike amplitude and relative bandwidth (right). These plots show that lower-frequency spikes are typically stronger, and stronger spikes tend to be more narrowband, though the correlation coefficients are somewhat low.

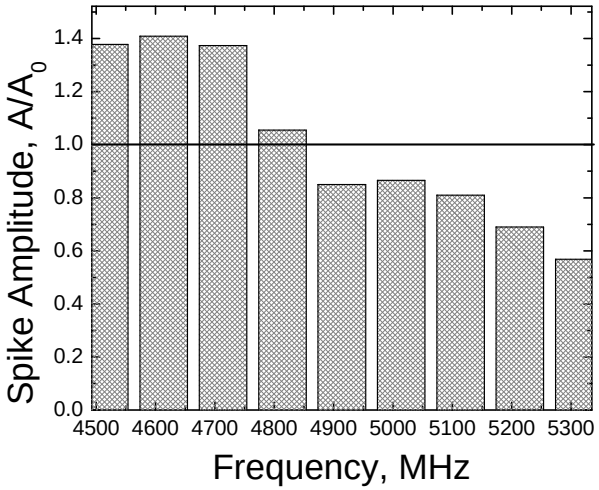

Fig. 10.— Moving average of spikes amplitudes vs. spike mean frequency. At least 100 spikes were averaged for each frequency range.

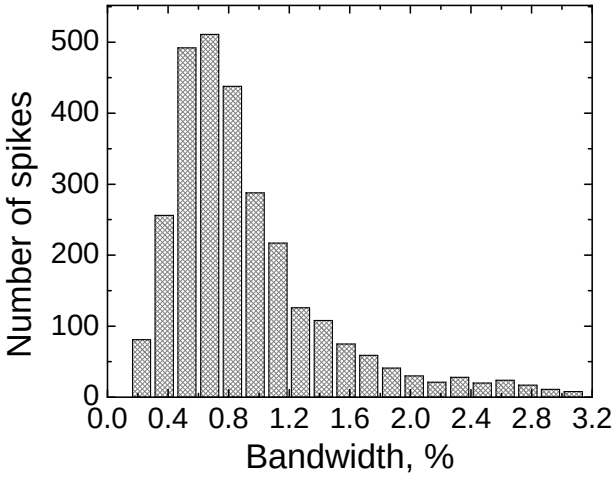

Fig. 11.— Bandwidth distribution of the extracted spikes. The binsize is taken to be 0.15% to avoid any coincidence with the spectral resolution of the instrument. Note prominent asymmetry of the distribution.

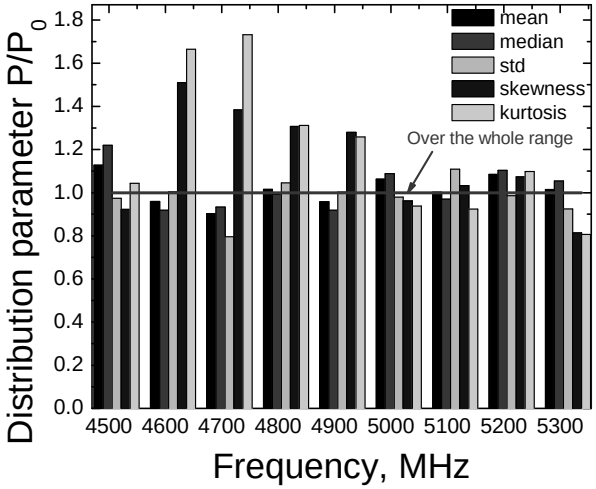

Fig. 12.— Parameters of the spikes bandwidth distribution versus spike mean frequency. For each frequency range the distributions were calculated over at least 100 spikes.

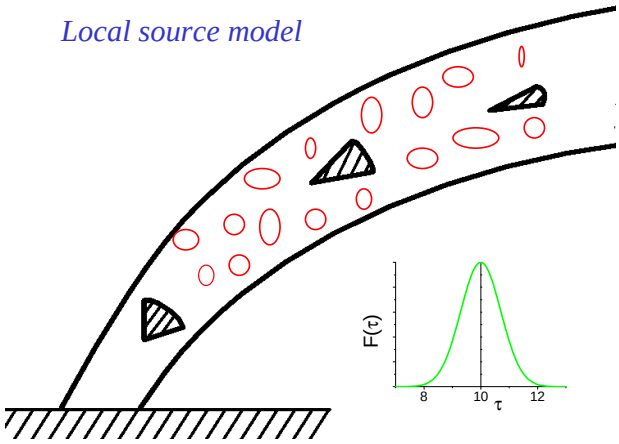

Fig. 13.— Sketch for the local trap model of spike generation. Red ovals show local traps where the pitch-angle anisotropy of the fast electron distribution is enhanced due to fluctuations of the magnetic field provided by magnetic turbulence in the large-scale trap. The inset displays the adopted symmetric (gaussian) distribution of the local spike sources over the ECM optical depth τ with the mean value $\tau = 10$ and dispersion $\sigma = 1$.

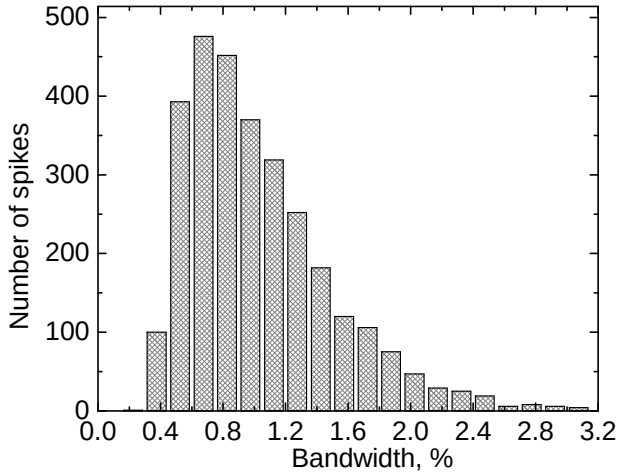

Fig. 14.— Spike bandwidth distribution obtained from the local trap model.

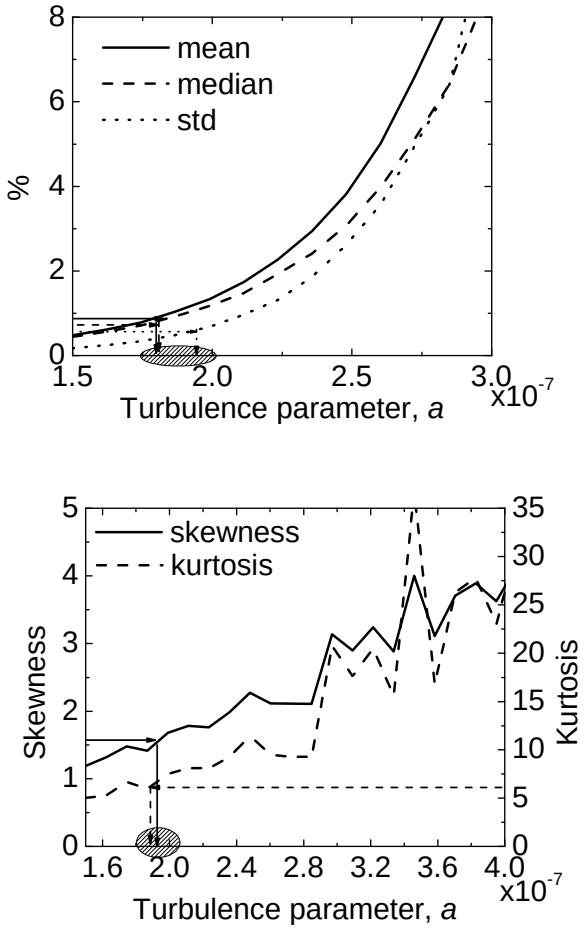

Fig. 15.— Dependences of the spike bandwidth distribution parameters on turbulence parameter a obtained from the local trap model described in the text.